Atmos. Meas. Tech., 8, 1863–1874, 2015
www.atmos-meas-tech.net/8/1863/2015/
doi:10.5194/amt-8-1863-2015

Atmospheric Measurement Techniques
Open Access

Zeeman effect in atmospheric O_2 measured by ground-based microwave radiometry

F. Navas-Guzmán[1], N. Kämpfer[1], A. Murk[1], R. Larsson[2], S. A. Buehler[3], and P. Eriksson[4]

[1]Institute of Applied Physics (IAP), University of Bern, Bern, Switzerland
[2]Division of Space Technology, Department of Computer Science, Electrical and Space Engineering, Luleå University of Technology, Box 812, 98128 Kiruna, Sweden
[3]Meteorological Institute, Center for Earth System Research and Sustainability, University of Hamburg, Germany
[4]Department of Earth and Space Sciences, Chalmers University of Technology, 41296 Gothenburg, Sweden

Correspondence to: F. Navas-Guzmán (francisco.navas@iap.unibe.ch)

Received: 18 November 2014 – Published in Atmos. Meas. Tech. Discuss.: 5 January 2015
Revised: 19 March 2015 – Accepted: 7 April 2015 – Published: 23 April 2015

Abstract. In this work we study the Zeeman effect on stratospheric O_2 using ground-based microwave radiometer measurements. The interaction of the Earth magnetic field with the oxygen dipole leads to a splitting of O_2 energy states, which polarizes the emission spectra. A special campaign was carried out in order to measure this effect in the oxygen emission line centered at 53.07 GHz. Both a fixed and a rotating mirror were incorporated into the TEMPERA (TEMPERature RAdiometer) in order to be able to measure under different observational angles. This new configuration allowed us to change the angle between the observational path and the Earth magnetic field direction. Moreover, a high-resolution spectrometer (1 kHz) was used in order to measure for the first time the polarization state of the radiation due to the Zeeman effect in the main isotopologue of oxygen from ground-based microwave measurements. The measured spectra showed a clear polarized signature when the observational angles were changed, evidencing the Zeeman effect in the oxygen molecule. In addition, simulations carried out with the Atmospheric Radiative Transfer Simulator (ARTS) allowed us to verify the microwave measurements showing a very good agreement between model and measurements. The results suggest some interesting new aspects for research of the upper atmosphere.

1 Introduction

The Zeeman effect is a phenomenon which occurs when an external magnetic field interacts with a molecule or an atom of total electron spin different from 0. Such an interaction will split an original energy level into several sublevels (Lenoir, 1967). In the atmosphere, oxygen is an abundant molecule which in its ground electronic state has a permanent magnetic dipole moment coming from two parallel electron spins. The interaction of the magnetic dipole moment with the Earth magnetic field leads to a Zeeman splitting of the O_2 rotational transitions. In this state, each rotational level with quantum number N is split into three levels of total quantum number J (J_J) following a Hund's coupling case (Pardo et al., 1995). This effect was studied by Gautier (1967) and Lenoir (1967, 1968) in the 60 GHz band of the main isotopologue $^{16}O_2$. It is established, from these works, that the Earth's magnetic field splits the different Zeeman components over a range of a few megahertz around the center of each rotational line. The shape of each component is governed by a pressure broadening mechanism up to 60 km of altitude and by a Doppler mechanism above (Pardo et al., 1995).

Zeeman splitting of millimeter-wavelength emissions of oxygen molecules must be taken into account for altitudes above 45 km in the terrestrial atmosphere when modeling the radiative transfer of these molecules. Temperature soundings of the atmosphere at high altitudes are not possible without including this effect (Von Engeln et al., 1998; Von Engeln and Buehler, 2002; Stähli et al., 2013; Shvetsov et al., 2010).

Observation of the Zeeman effect from ground-based measurements was first performed by Waters (1973) for atmospheric O_2 at 53 GHz. Pardo et al. (1995) were able to measure the Zeeman substructure for atmospheric $^{16}O^{18}O$ at 233.95 GHz. For this rare isotopic species the relative abundance is much lower than for ^{16}O molecule, and its emission from upper atmospheric layers can be observed and the Zeeman substructure detected from the ground (Pardo et al., 1995). The main difficulty for observations of the Zeeman structure of ^{16}O molecule comes from its very broad tropospheric emission and the high opacity of low layers which eliminate any structure.

The observation of this effect for ^{16}O has also been possible from satellite measurements. Hartmann et al. (1996) observed the Zeeman broadening of the oxygen emission line of the 9^+ line in the 61.1509 ± 0.062 GHz frequency range using the Millimeter-Wave Atmospheric Sounder on the NASA space shuttle during the ATLAS missions. Comparison of satellite measurements and radiative transfer models including the Zeeman effect have also been addressed (Han et al., 2007, 2010; Schwartz et al., 2006). Han et al. (2007) used spectral passband measurements from the Special Sensor Microwave Imager/Sounder (SSMIS) on board the Defense Meteorology Satellite Program F-16 satellite to measure the oxygen magnetic dipole transitions (7+, 9+, 15+, and 17+; Rosenkranz, 1993). These measurements were used to validate a fast model developed from the radiative transfer model of Rosenkranz and Staelin (1988). Moreover, the measurements were also used together with data from the Microwave Limb Sounder (MLS) on board the Aura spacecraft for assimilation in a numerical weather prediction (NWP) model (Hoppel et al., 2013). Schwartz et al. (2006) also reported a comparison of another radiative transfer model with measurements of the 118 GHz oxygen line from MLS.

In this work we present an experiment in which the Zeeman broadening of the oxygen emission line at 53.0669 GHz is observed and the polarization state of the radiation due to this effect is detected for the first time using a ground-based microwave radiometer.

The measurements were possible using a fast Fourier transform (FFT) spectrometer with 1 GHz of bandwidth to measure the whole oxygen emission line centered at 53.07 GHz and a narrow spectrometer (4 MHz) to measure the center of the line with a very high resolution (1 kHz). These measurements have been compared to a model which includes the Zeeman-splitting effect. The incorporation of this effect to the forward model will allow extension to the temperature retrievals beyond 50 km. This improvement in the forward model will be very useful for the assimilation of brightness temperatures in NWP models. It is also important to note that ground-based measurements of the atmosphere with good temporal resolution complement satellite measurements, which are temporally limited by their satellite's orbital parameters.

The paper is organized as follows: in Sect. 2, the instrumentation and the measurements are briefly outlined. The Zeeman effect theory and the modeling are presented in Sect. 3. Section 4 presents the results of this study. Firstly the simulations using a model are addressed and secondly the tropospheric correction performed to the radiometer measurements and the results obtained during this campaign are presented. Finally, the conclusions are given in Sect. 5.

2 Instrumentation and measurements

The TEMPERA (TEMPERature RAdiometer) radiometer is a microwave radiometer that provides temperature profiles from the ground to around 50 km (Stähli et al., 2013). This is the first microwave radiometer that measures temperature in the troposphere and stratosphere at the same time. The instrument is a heterodyne receiver at a frequency range of 51–57 GHz. Figure 1 shows a picture of TEMPERA, which is operated in a temperature-stabilized laboratory in the ExWi building of the University of Bern (Bern, Switzerland; 575 m above sea level; 46.95° N, 7.44° E). In this lab a styrofoam window allows views of the atmosphere over the zenith angle range from 30 to 70°. The instrument mainly consists of three parts: the front end to collect and detect the microwave radiation and two back ends consisting of a filter bank and a digital FFT spectrometer for the spectral analysis. The radiation is directed into the corrugated horn antenna using an off-axis parabolic mirror. The antenna beam has a half power beam width (HPBW) of 4°. The signal is then amplified and down-converted to an intermediate frequency for further spectral analysis. A noise diode in combination with an ambient hot load is used for calibration in each measurement cycle. The noise diode is calibrated regularly (about once a month) using a cold load (liquid nitrogen) and a hot load (ambient). The receiver noise temperature T_N is in the range from 475 to 665 K. More details about the calibration with TEMPERA can be found in Stähli et al. (2013).

For tropospheric measurements the instrument uses a filter bank with four channels. By switching the local oscillator frequency with a synthesizer, it is possible to measure at 12 frequencies. In this way TEMPERA covers uniformly the range from 51 to 57 GHz at positions between the emission lines. Tropospheric retrievals are not addressed in this paper and more details about this measurement mode can be found in Stähli et al. (2013) and Navas-Guzmán et al. (2014).

The second back end is used for stratospheric measurements and contains a digital FFT spectrometer (Acqiris AC240) for the two emission lines centered at 52.5424 and 53.0669 GHz. The FFT spectrometer measures the two emission lines with a resolution of 30.5 kHz and a bandwidth of 960 MHz. The receiver noise temperature T_N for the receiver–spectrometer combination is around 480 K. An overview of the technical specifications is given in Table 1.

An example of FFT measurements is shown in Fig. 2 (upper panel). This figure shows the brightness temperature on

Table 1. Specifications of TEMPERA.

Optical system	Corrugated horn antenna with parabolic mirror, HPBW = 4°
Receiver type	Uncooled heterodyne receiver, filter bank; digital FFT spectrometer
RF frequency range	Filter bank: 51–57 GHz, FFT spectrometer: 52.4–53.2 GHz
Receiver operation	Single sideband mode
Receiver noise temperature	475–665 K
Filter bank	Four filters, bandwidth 250 MHz and 1 GHz
FFT spectrometer	Bandwidth 1 GHz, resolution 30.5 kHz, 32 768 channels
Mixer (FFT back end)	I/Q
Calibration	Hot load, noise diode

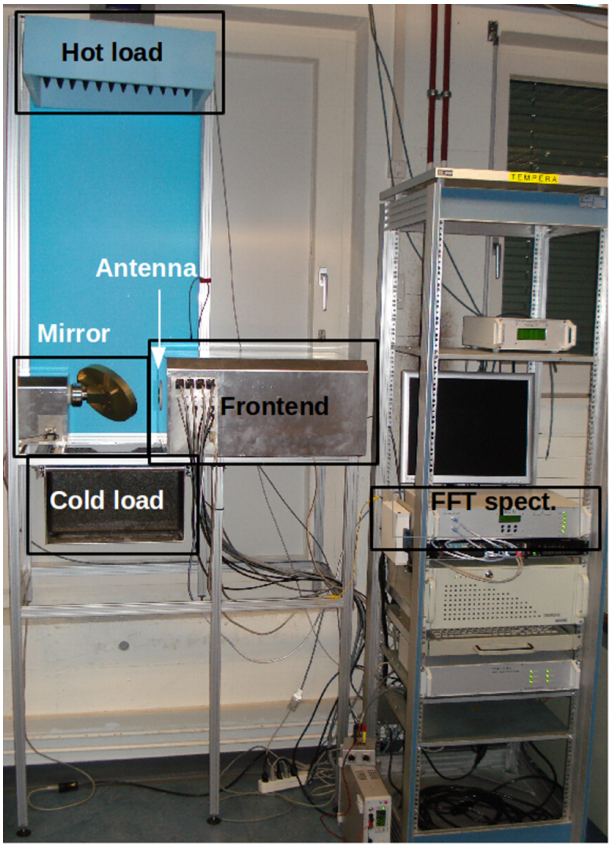

Figure 1. TEMPERA at the laboratory at ExWi, Bern (Switzerland).

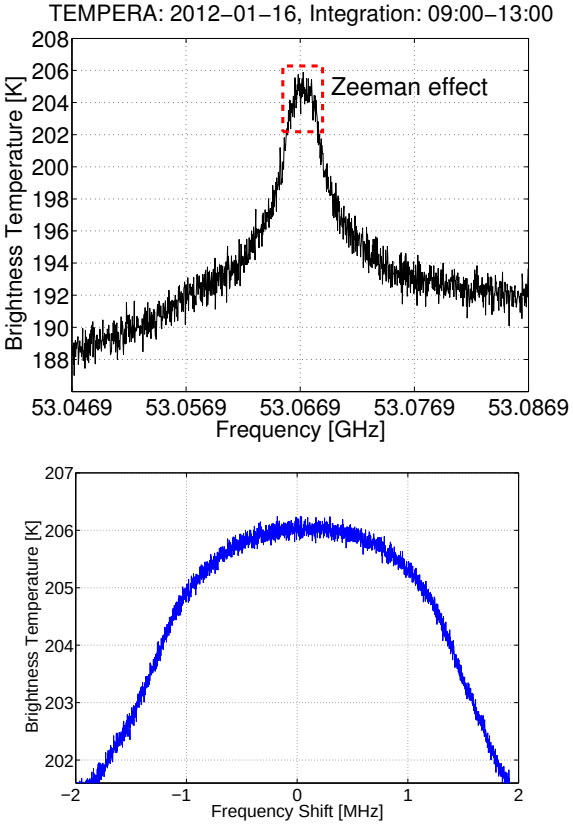

Figure 2. Upper panel: brightness temperature spectrum measured with the FFT spectrometer in the oxygen emission line of 53.07 GHz. The red box indicates the broadened line shape due to the Zeeman effect. Lower panel: monthly mean brightness temperature spectrum measured with the SDR spectrometer.

16 January of 2012 for the oxygen emission line centered at 53.07 GHz. The red box indicates the influence of the Zeeman effect by the broadened line shape in the center with a kind of a plateau (round line shape around the line center: ±1 MHz).

A second spectrometer was installed in TEMPERA in order to measure with a higher resolution the narrow spectral region where a broadening in the oxygen emission line is produced due to the Zeeman effect. This narrow-band software defined ratio (SDR) spectrometer consists of 4096 channels which cover a bandwidth of 4 MHz with a resolution of 1 kHz. An example of a monthly mean brightness temperature spectrum centered at 53.07 GHz measured with the SDR spectrometer is shown in Fig. 2 (lower panel).

Moreover, a set of two auxiliary mirrors was installed on the roof of the ExWi building in the University of Bern (Fig. 3). A rotating mirror allows one to observe the atmosphere under different azimuth angles and with a fixed elevation angle, while the fixed mirror directs the radiation from the rotating mirror into TEMPERA radiometer. The

Figure 3. Secondary mirror installed on the roof of the ExWi building at the University of Bern.

main goal of using these auxiliary mirrors is to measure the Zeeman-broadened oxygen line under different angles relative to the Earth's magnetic field.

A special campaign was carried out in autumn of 2013 in order to detect the Zeeman effect with TEMPERA. Three months of measurements (September–November 2013) were performed using these auxiliary mirrors and the SDR spectrometer. A special measurement cycle was designed for TEMPERA during this period. Periodic cycles of almost 5 min were performed. This whole cycle consisted of 13 subcycles, each one starting with a hot load calibration in combination with a noise diode for 10 s followed by other 10 s of atmospheric measurements in one azimuth direction. A total of 13 azimuth angles were scanned ranging from 71.5 to 191° in steps of 10° during the whole cycle. The elevation angle was fixed at 60° during all the measurements since it was found as the angle at which the intensity of the emission lines was highest (Stähli et al., 2013).

3 Zeeman effect theory and modeling

3.1 Theory

The Zeeman effect (Zeeman, 1897) occurs because the spin of unpaired electrons couples to the external magnetic field, changing the internal energy of the molecule. A transition between two of these altered energy levels can change the frequency dependence of the absorption spectrum. The Zeeman energy change is calculated by

$$\Delta E = -g\mu_0 M\ |\boldsymbol{H}|, \tag{1}$$

where g depends on the line and molecule (see, e.g., Christensen and Veseth (1978) for molecular oxygen), μ_0 is the Bohr magneton, $M(J_{\mathrm{M}})$ is the projection of J on the magnetic field, and $\boldsymbol{H}$ is the magnetic field vector. The quantum numbers necessary can be found in most databases, e.g., HITRAN (Rothman et al., 2013). There are $2J+1$ possible M for a state level (these are $M = -J, -J+1, \cdots, J-1, J$), and M can only change by 0 or ± 1. A transition without changing the value of M is called a π transition, and a transition with changing M is called a $\sigma_{\pm}$ transition. The total line strength is not altered by the effect but will be distributed among the new lines. Each line "produced" by this procedure then undergoes the same broadening mechanisms (thermal and pressure) to create the absorption spectrum.

In addition to splitting the line, the change in energy level depends on the direction of the magnetic field and the propagation path of the radiation, which means that the absorption also depends on the polarization of the radiation. The main polarization occurs along the magnetic field in the plane perpendicular to the propagating radiation. If $\boldsymbol{H}$ is entirely in this plane, then the radiation will be linearly polarized along $\boldsymbol{H}$ for $\sigma_{\pm}$ transitions and linearly polarized perpendicular to $\boldsymbol{H}$ for π transitions. If $\boldsymbol{H}$ is parallel/anti-parallel to the path of the propagating radiation, then the σ_+ and σ_- transitions will circularly polarize the radiation in opposite ways, and π transitions do not affect the radiation at all. The polarizing effect will generally scale between the two cases above as a function of the angle that $\boldsymbol{H}$ forms with the direction of the propagating radiation.

3.2 Modeling

The first official release of the Atmospheric Radiative Transfer Simulator (ARTS) was by Buehler et al. (2005) as a flexible/modular code base for radiative transfer simulations. Since then, ARTS has been under continual development. One key release is version 2.0 by Eriksson et al. (2011), which describes the ARTS scripting potential and a few of the modules. Presently, ARTS is at version 2.2; the latest version includes, among other new features, a module that calculates the Zeeman effect presented by Larsson et al. (2014).

In short, ARTS calculates each of the three polarization components individually before adding their absorption contributions to a Stokes vector propagation matrix. The polarization of the radiation is internally kept in a universal coordinate system defined by the sensor through all of the propagation. The line shape should return both its imaginary and real part to account for dispersion-caused polarization rotation. The input magnetic field is either static or three 3-D-gridded fields, one field for each coordinate: x, y, and z. This propagation matrix is then sent to the radiative transfer calculator, which solves the vector radiative transfer equation (as

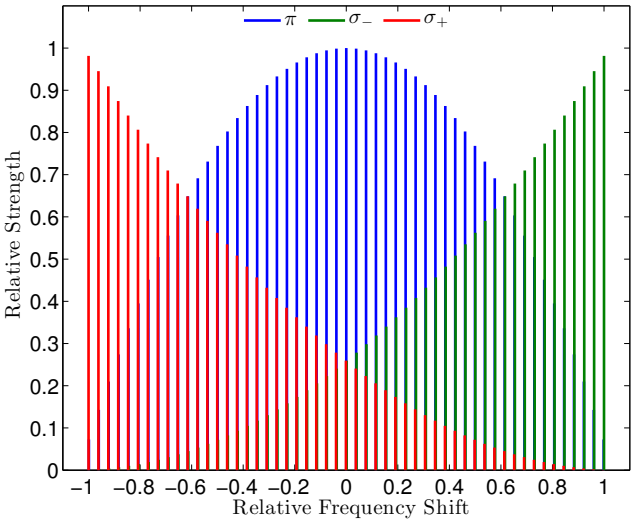

Figure 4. Example of Zeeman pattern for the 53 GHz $^{16}O_2$ line that is observed by TEMPERA. The colors represent the Zeeman component as indicated by the legend. The plot is renormalized on both axes as described in the text.

in, e.g., del Toro Ininiesta, 2003)

$$\frac{\mathrm{d}\boldsymbol{I}}{\mathrm{d}\boldsymbol{r}} = -\mathbf{K}(\boldsymbol{I} - \boldsymbol{B}), \quad (2)$$

where $\boldsymbol{I}$ is the Stokes vector, $\boldsymbol{r}$ is the path vector, $\mathbf{K}$ is the propagation matrix, and $\boldsymbol{B}$ is the Stokes version of Planck's function for blackbody radiation. For details on the ARTS Zeeman effect module see Larsson et al. (2014).

The calculated relative Zeeman pattern for the line measured by TEMPERA can be found in Fig. 4. This otherwise singular line is split into 159 Zeeman lines, 53 for each polarization component. The plot has been renormalized for readability. The strongest split line accounts for less than 1.5 % of the original strength of the line, the maximum splitting from the central line is $\sim 27.99\,\mathrm{kHz\,\mu T^{-1}}$, and the splitting between the individual lines is about $1.08\,\mathrm{kHz\,\mu T^{-1}}$ within a component. The last number is significantly small. The thermal broadening in the stratosphere is under normal conditions larger than the magnetic line splitting above Bern, so individual Zeeman lines cannot be discerned from the overall shape.

4 Results

4.1 Brightness temperature simulations incorporating the Zeeman effect

Brightness temperature spectra have been simulated using the ARTS model which was described in the previous section. ARTS was set with all the information about instrumental aspects and location of TEMPERA in order to simulate the same measurement conditions. The brightness temperature was calculated for 13 azimuth angles (71.5 : 10 : 191.5°) and a fixed elevation angle (60°) and to simulate the atmospheric conditions of 15 October 2013 (Figs. 5 and 6). The altitude of the platform was set at 12 km in order to avoid any tropospheric effect in the spectra. On 15 October 2013, the total intensity of the magnetic field over Bern at the altitude of 50 km was 46 547 nT with a declination of 1°21′44″ and an inclination of 62°46′16″ (www.ngdc.noaa.gov/geomag/magfield.shtml). Figure 5 shows the calculated brightness temperature spectra for a linear horizontal polarization of the oxygen emission line centered at 53.07 GHz in a range of 5 MHz. From these simulations we can observe that the spectra are almost identical for most of the frequency range plotted here and differences are only observed in the central part when the observational azimuth angle is changed. In the narrow central frequency range we can observe that both the shape and the intensity of the spectra changes for the different observations. For the higher azimuth angles the brightness temperature spectra are lower and the shape is flatter, while for lower angles the spectra are higher and the shape is less flat. The maximum difference in brightness temperature between the most intensive spectrum (91.5°) and the least intensive (191.5°) is 2.5 K. Figure 6 shows linear vertical polarization. We observe a similar pattern for linear vertical polarization as for linear horizontal polarization, with the peak strength of the signal changing mostly in the center of the line as a function of the azimuthal angle. However, the change is much smaller for linear vertical polarization, which only has a maximum difference of 1 K between the most and least intense spectra. Also, the change with azimuthal angle is inverted compared to linear horizontal polarization. For the linear vertical polarization the most intensive spectrum corresponds to the observational angle of 181.5° while the least intensive corresponds to 91.5°. This behavior is clearly associated with the polarized nature of the Zeeman effect, since the polarized state of the observed radiation changes when the angle between the propagation path and the direction of the Earth magnetic field is varied. It is also interesting to note from Figs. 5 and 6 that the differences between horizontal and vertical polarization are very small when close to the 181° azimuth angle. This is in good agreement with theory, as this direction corresponds to measurements of radiation which has been propagated along the magnetic field towards TEMPERA. This parallel propagation results in minimal differences among linear polarizations.

The brightness temperature has also been simulated without considering the Zeeman effect in the ARTS model. These simulations correspond to the dashed lines shown in Figs. 5 and 6. We found that when the Zeeman module is not active there is no difference in the spectra for difference observational angles. Moreover, the spectrum presents higher brightness temperature values and it does not show any broadening in the center of the oxygen emission line.

In order to compare the simulated spectra from ARTS with the measurements, the effects of the different optical components of TEMPERA on the polarization state of the radiation,

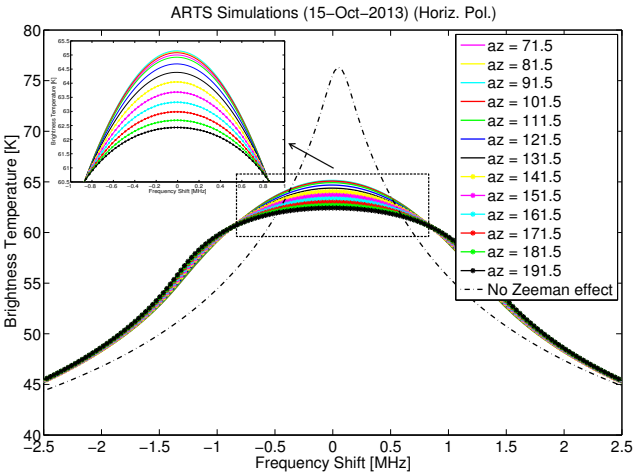

Figure 5. Simulated horizontally polarized spectra on 15 October 2013 with (continuous lines) and without (dashed line) the Zeeman effect.

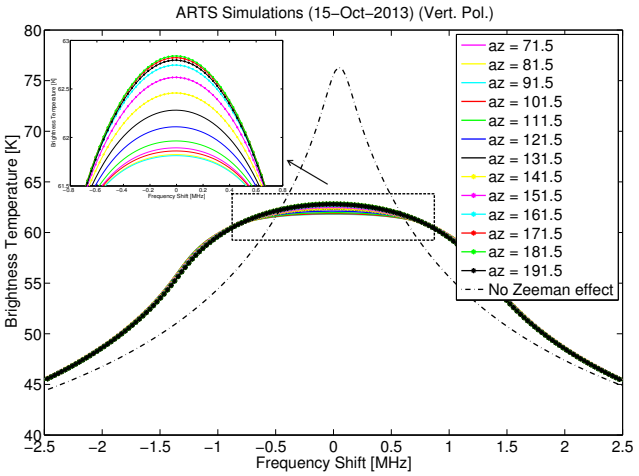

Figure 6. As in Fig. 5 but considering vertical polarization.

as well as the vertically polarized observing antenna, have to be considered. A full characterization of the polarization state of the radiation can be done by means of the Stokes vector, $\boldsymbol{s}$, which is defined as

$$\boldsymbol{s} = \begin{bmatrix} I \\ Q \\ U \\ V \end{bmatrix} = \frac{1}{2}\sqrt{\frac{\varepsilon}{\mu}} \begin{bmatrix} \langle E_\mathrm{v} E_\mathrm{v}^* + E_\mathrm{h} E_\mathrm{h}^* \rangle \\ \langle E_\mathrm{v} E_\mathrm{v}^* - E_\mathrm{h} E_\mathrm{h}^* \rangle \\ \langle E_\mathrm{v} E_\mathrm{h}^* - E_\mathrm{h} E_\mathrm{v}^* \rangle \\ \langle E_\mathrm{h} E_\mathrm{v}^* - E_\mathrm{v} E_\mathrm{h}^* \rangle \end{bmatrix}, \tag{3}$$

where ε and μ are the electric and magnetic constants, respectively, $< \cdot >$ indicates time average, and E_v and E_h are the complex amplitudes for vertical and horizontal polarization. The first Stokes component (I) is the total intensity, the second component (Q) is the difference between vertical and horizontal polarization, and the last two components, U and V, correspond to linear $\pm 45°$ and circular polarization, respectively. The Stokes components are converted to brightness temperature by inverting the Planck function (Eriksson et al., 2011); this new Stokes vector of brightness temperatures is denoted as $\mathbf{s}'$.

The calculus of the measured brightness temperature (T_b^p) considering the sensor polarization response can be expressed as (cf. Eriksson et al. (2011), Eq. 19)

$$T_\mathrm{b}^\mathrm{p} = \boldsymbol{p}\mathbf{L}(\chi)\mathbf{s}', \tag{4}$$

where $\boldsymbol{p}$ is a row vector of length 4 which describes the sensor polarization response. In the case of TEMPERA, whose antenna is vertically polarized, the vector $\boldsymbol{p}$ is [1100]. The rotation of the Stokes reference frame due to the reflection in the different mirrors and the rotation of the external mirror is considered using the transformation matrix $\mathbf{L}(\chi)$, which allows one to obtain a consistent definition between the polarization directions for atmospheric radiation and sensor response. This matrix is defined as (Liou, 2002)

$$\mathbf{L}(\chi) = \begin{bmatrix} 1 & 0 & 0 & 0 \\ 0 & \cos 2\chi & \sin 2\chi & 0 \\ 0 & -\sin 2\chi & \cos 2\chi & 0 \\ 0 & 0 & 0 & 1 \end{bmatrix}. \tag{5}$$

The rotational angle (χ) has been calculated using the GRASP software package (www.ticra.com/products/software/grasp). This software package allows design and analysis of complex reflector elements using physical optics, physical theory of diffraction and the method of moments. Figure 7 shows the setup of this simulation, where we can see the different TEMPERA components (horn antenna, parabolic mirror and the two auxiliary mirrors, the fixed and the rotating mirror) and the ray tracing of an electric field which is propagated from the antenna to the atmosphere. The calculated angle χ can be expressed as $\chi = \varphi + \varphi_\mathrm{offset}$, where φ is the observational azimuth angle defined in our experiments ($\varphi = 71.5 : 10 : 191.5°$) and φ_offset is 141.5°. Once the sensor polarization response and the rotation of the polarized radiation have been characterized, the effective brightness temperature can be calculated as (Eriksson et al., 2006)

$$T_\mathrm{b}^\mathrm{p} = [1100]\mathbf{L}(\chi)\mathbf{s}'. \tag{6}$$

Figure 8 shows the effective brightness temperature spectra calculated for the case simulated in ARTS (15 October 2013) in Figs. 5 and 6. For these spectra we can appreciate again the same pattern as in the ARTS simulations, with almost the same intensity on the wings of the oxygen emission line and some differences in the central frequencies when the azimuth angle is changed. The highest brightness temperature is found at 71.5°, while the lowest is found at 191.5°. The latter position corresponds to the maximum broadening found when the direction of observation is almost antiparallel to the direction south–north. The maximum difference between the most and the least intense spectra is 2.5 K.

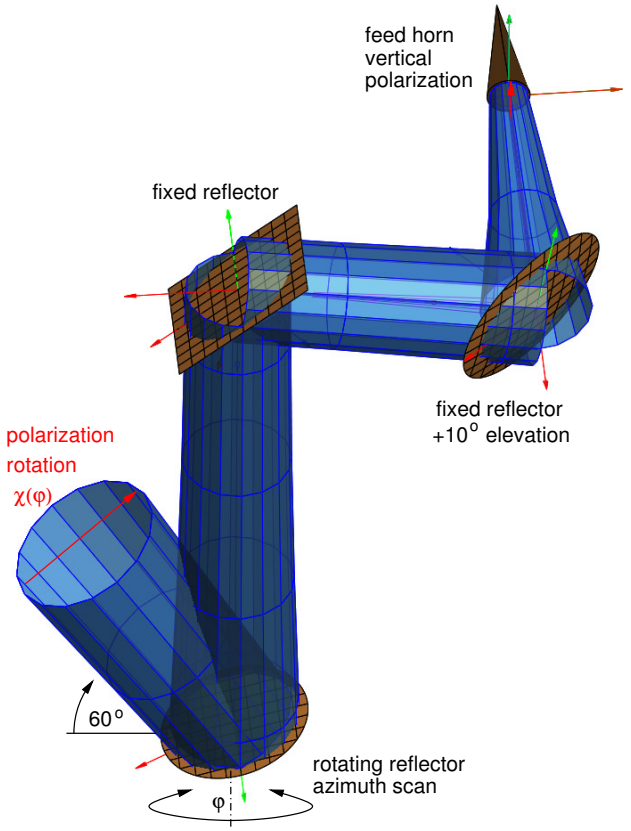

Figure 7. Simulation of the propagation of a vertical electric field from the TEMPERA antenna to the atmosphere and passing through the different mirrors using the GRASP package software.

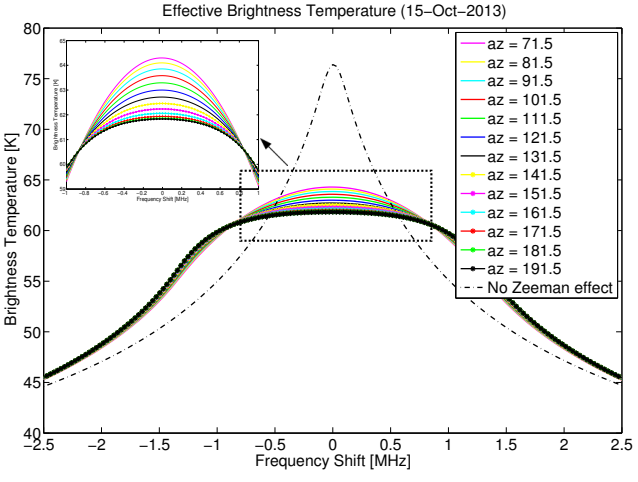

Figure 8. Simulated effective brightness temperature, taking into account that the radiation passed through the different TEMPERA components.

In order to study the difference in the broadening of each azimuth observational spectrum due to the Zeeman effect, we have calculated the ratio among each spectrum to the

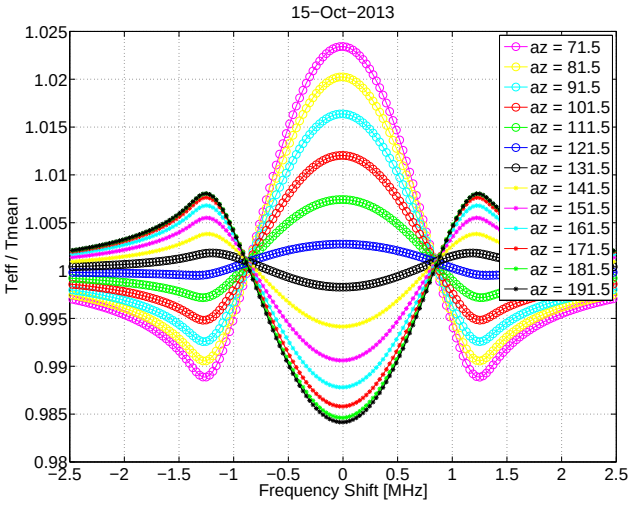

Figure 9. Ratio between the effective temperature for each observational angle and the averaged spectra for ARTS simulations.

averaged spectrum from all the observational angles. Figure 9 shows these ratios for the different azimuth angles. Azimuthal behavior with a ratio below unity in the center of the line also has a ratio above unity in the wings, which means that the line experienced more than average broadening. The opposite is also true: azimuthal behavior with values above unity in the center means less than average broadening. The different ratios show a clear azimuth dependence, indicating that the highest broadening is found when the azimuth angle is 191.5° while the smaller broadening is found at 71.5°.

4.2 Tropospheric correction of SDR spectrometer

A ground-based microwave radiometer measures a superposition of emission and absorption of radiation at different altitudes. The received intensity at ground level can be expressed in the Rayleigh–Jeans limit ($h\upsilon \ll kT$) as a function of the brightness temperature. In these conditions the radiative transfer equation is given by

$$T_\mathrm{b}(\upsilon, z_0) = T_0 e^{-\tau(\upsilon, z_1)} + \int_{z_0}^{z_1} T(z) e^{-\tau(\upsilon, z)} \alpha(\upsilon, z) \mathrm{d}z, \qquad (7)$$

where T_b is the brightness temperature at frequency υ, T_0 is the brightness temperature of the cosmic background radiation, $T(z)$ is the physical temperature at height z, z_0 is the Earth surface, z_1 is the upper boundary in the atmosphere, α is the absorption coefficient, and τ is the opacity. The opacity is defined as

$$\tau(\upsilon, z) = \int_{z_0}^{z} \alpha(\upsilon, z') \mathrm{d}z'. \qquad (8)$$

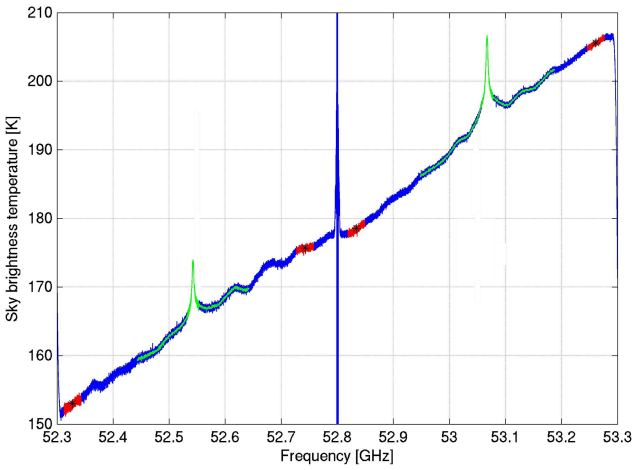

Figure 10. Example of calibrated spectrum of the FFT spectrometer. The frequency ranges marked in red are the areas used for the correction of tropospheric attenuation. The mean value of each range, indicated by a black star, is the value used for the correction.

The contribution of the troposphere to the brightness temperature measured with a microwave radiometer at ground level is very important and it could be very different depending on the observational direction or on the period of measurements. After oxygen, water vapor and liquid water (clouds) are the most important components in the atmosphere, the emissions of which have relevance in the microwave spectrum. It is very important to correct our measurements for any tropospheric effect in order to ensure that the changes observed in our measurements for different observational directions come from the stratosphere (Zeeman effect) and not from the troposphere.

Since the tropospheric portion of the pathlength provides a relatively spectrally flat signal the microwave radiative transfer equation can be rewritten as

$$T_b(z_0) = T_b(z_{trop})e^{-\tau} + T_{trop}(1 - e^{-\tau}), \quad (9)$$

where $T_b(z_{trop})$ is the brightness temperature as observed from the tropopause, τ is the tropospheric zenith opacity, and T_{trop} is the effective temperature of the troposphere.

From this equation the opacity can be calculated as

$$\tau = -\ln\left(\frac{T_{trop} - T_b(z_0)}{T_{trop} - T_b(z_{trop})}\right). \quad (10)$$

Since the atmospheric opacity is dominated by the contribution from the troposphere, the stratospheric contribution is considered negligible and the cosmic background radiation, T_{bg}, is in practice used instead of $T_b(z_{trop})$ in Eq. (10). This means that the calculated τ actually is approximately the total atmospheric opacity and hence includes the minor contribution from altitudes above the troposphere (e.g., absorption by stratospheric O_2 and H_2O) (Forkman et al., 2012).

T_{trop} has been estimated using a linear model between the weighted tropospheric temperature and the ground temperature (Ingold et al., 1998). The weighted tropospheric temperature was calculated using radiosonde measurements. Radiosondes are launched twice a day at the aerological station of MeteoSwiss in Payerne (40 km west of Bern). One year of radiosonde data was used and the linear fit found between T_{trop} at 53 GHz and the ground temperature T_{z_0} was $T_{trop} = 0.8159T_{z_0} + 47.21$ K. The constant term T_{bg} is independent of frequency and has a value of 2.7 K (Gush et al., 1990). The term $T_b(z_0)$ is measured using the wings of the oxygen emission line centered at 53.07 GHz for every azimuth angle. The simultaneous measurements performed with the FFT spectrometer allow us to measure in the wings of the oxygen emission line, where most of the contribution to the brightness temperature comes from the troposphere. In the frequency range of interest, the tropospheric attenuation increases with increasing frequency. In order to account for this, we determine the correction factor at each frequency using a linear fit between the frequency ranges highlighted in red in Fig. 10.

Once all the terms are calculated, the brightness temperature corrected for tropospheric effects can be obtained as

$$T_b(z_{trop}) = \frac{T_b(z_0) - T_{trop}(1 - e^{-\tau})}{e^{-\tau}}. \quad (11)$$

It is interesting to note that for the correction presented in this section we have used the scalar radiative transfer equation, since this tropospheric correction is independent of polarization state. This assumption is valid if scattering can be neglected, which should hold in the absence of strong precipitation.

4.3 Stratospheric brightness temperature measurements

As already described in Sect. 2, a special campaign of microwave radiometer measurements has been performed for 3 months in autumn 2013 in the ExWi building of University of Bern. During this campaign, TEMPERA was set with a special configuration in order to be able to observe the Zeeman effect from ground-based measurements. Radiometer measurements in different azimuth angles (13 angles) were carried out in order to scan the atmosphere under different angles between the propagation path and the local Earth magnetic field. Figure 11 shows mean monthly brightness temperature spectra obtained for different azimuth angles in October 2013. All the measurements were corrected for tropospheric effects following the procedure described in the previous section. Figure 11a shows the whole range (4 MHz) measured with the SDR spectrometer. From this plot we observe that the mean spectra for the different azimuth angles show almost identical values outside of the narrow central region. However, differences in the intensity and

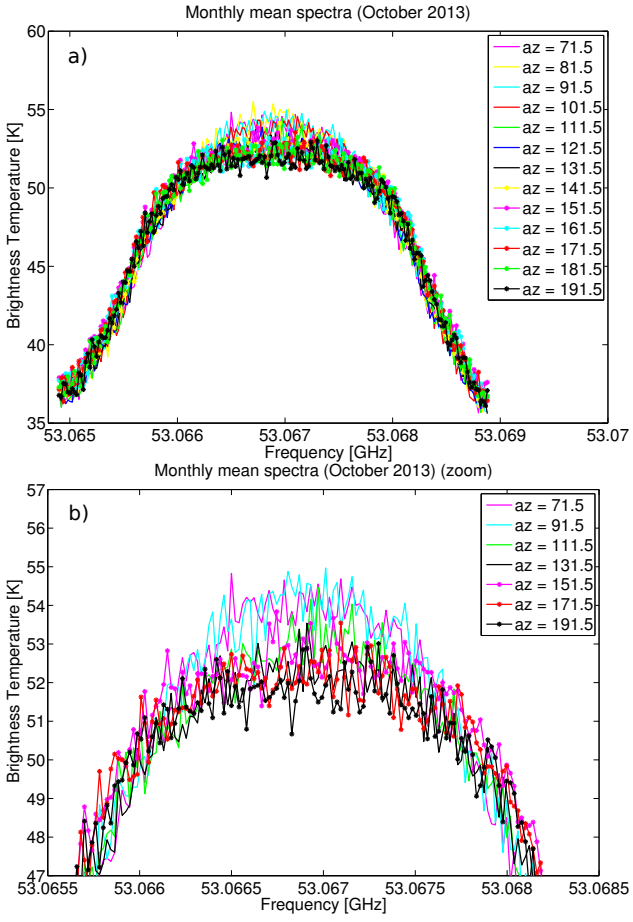

Figure 11. Monthly brightness temperature from SDR corrected for tropospheric effects (October 2013).

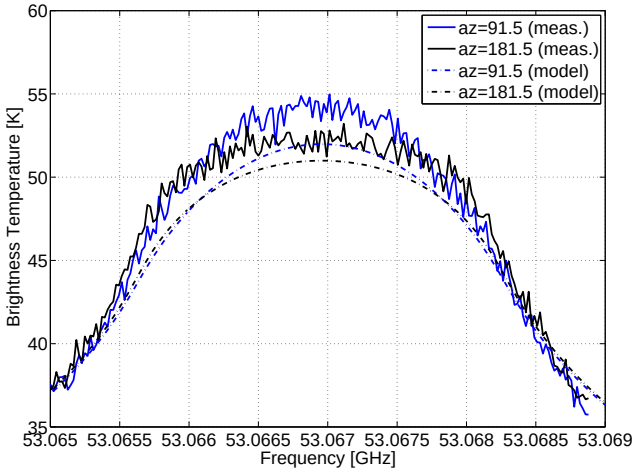

Figure 12. Brightness temperature spectra from the SDR spectrometer (solid lines) and simulated from ARTS (dash lines) for two different observational angles.

in the shape are observed in the very narrow range centered on 53.067 GHz. Figure 11b shows a zoom of the spectra in the central frequencies for some selected azimuth angles. We can observe that for higher azimuth angles the spectra show lower values of brightness temperature and flatter shapes in the central frequency range (±0.5 MHz), while higher brightness temperature and less flat shapes are observed in lower azimuth angles.

These results are in good agreement with the simulations performed including the Zeeman effect with ARTS (Sect. 4.1). However, we can notice that there is an offset in the brightness temperature spectra from model (highest peak ∼ 64 K) and from measurements (highest peak ∼ 54 K). The offset could be due to an inappropriate consideration of the continuum absorption from secondary species (water vapor, ozone, etc.) in the forward model and the fact that the contribution from line mixing to the oxygen spectra is not modeled. Other reasons that could explain some differences could be related to the uncertainties of the tropospheric correction in the measurements and to the fact we are comparing different periods of measurements: 1 day for the simulations (15 October 2015) and 1 month of integrated measurements (October 2013). In any case, while the baseline offset affects the absolute difference between model and data, the shape of the center line (±2 MHz) is not altered. Thus the main conclusions of Zeeman polarization measurements and the ARTS module validation are solid.

Figure 12 shows a direct comparison of the brightness temperature spectra from SDR measurements (solid lines) and from ARTS model (dashed lines) for two observational azimuth angles (91.5 and 181.5°). An offset correction has been applied to the simulated spectra in order to compare with the measurements. Although the absolute values are not exactly the same for the modeled and measured spectra in the center of the oxygen emission line we can clearly observe that the behavior of the spectra for the two azimuth angles are the same. The spectra show a higher broadening for the highest azimuth angle for both measurements and simulations. In order to compare the measurements with the model in a more quantitative way, we have compared the ratio of the maximum mean brightness temperature of each spectrum to the mean value for all the spectra at the central frequencies (range of ±0.25 MHz). Equation (12) indicates explicitly the expression of these calculations:

$$\frac{T_{\mathrm{eff}}(\max)}{T_{\mathrm{mean}}(\max)} = \frac{\mathrm{mean}[T_{\mathrm{b}}(\upsilon_1 - \upsilon_2, \psi_i)]}{\mathrm{mean}[\frac{\sum_{i=1}^{n_{\mathrm{t}}} T_{\mathrm{b}}(\upsilon_1 - \upsilon_2, \psi_i)}{n_{\mathrm{t}}}]}, \quad (12)$$

where υ_1 and υ_2 indicate the frequency range which corresponds to an interval of 0.5 MHz centered at 53.067 GHz. ψ_i is the observational azimuth angle for a specific position and n_{t} is the total number of positions scanned by TEMPERA (13 positions).

Figure 13 shows these ratios calculated with the ARTS model simulating the conditions of 15 October 2013 and the ones obtained from the mean monthly spectra (October 2013)

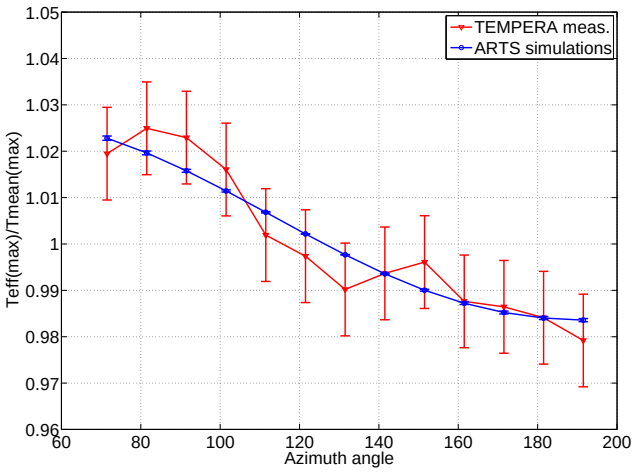

Figure 13. Ratios of maximum brightness temperature of each spectrum to the mean value for all the spectra at the central frequencies for TEMPERA radiometer (red points) and ARTS (blue points).

measured by TEMPERA. We can observe that, in general, there is a very good agreement between the measurements and the model. Both simulations and measurements show higher ratio values (> 1), which indicate a smaller broadening regarding the averaged spectrum for the smallest azimuth angles and a larger broadening (ratios < 1) for the largest angles. The relative differences between both ratios are lower than 1 % for all the azimuth angles. We observe that the ratios for some azimuth angles are almost identical while some discrepancies are observed for other ones. The errors for the TEMPERA measurements have been estimated by evaluating the uncertainties associated with the different terms of the tropospheric correction (Eq. 11). The error bars shown in Fig. 13 have been calculated using error propagation theory and they presented values very similar (~ 0.01) for all the observational angles. The errors associated with the simulations were obtained by evaluating the ratio of the simulated spectra plus Gaussian white noise. The calculated uncertainties presented values much smaller than the ones found for the measurements (maximum value of 4.6×10^{-4}). It is important to note that the differences found between measurements and simulations are within the measurement uncertainties. From this comparison we can conclude that the agreement between measurements and model is clear. These results show the polarized state of the radiation due to the Zeeman effect, which is revealed for a different broadening in the spectra when the angle of the Earth magnetic field and the observational path is changed.

5 Conclusions

This work presents an experiment in which the Zeeman broadening of the oxygen emission line at 53.0669 GHz is observed and the polarization state of the radiation due to this effect is detected for the first time using a ground-based microwave radiometer. A special campaign was carried out in order to detect this effect with the TEMPERA radiometer. The installation of a fixed and a rotating mirror in front of TEMPERA allowed us to measure under different angles between the observational path and the Earth's magnetic field direction. A total of 13 azimuth angles were scanned ranging from 71.5 to 191.5°. In addition, the use of a narrow spectrometer (4 MHz) allowed us to measure the center of the oxygen emission line with a very high resolution of 1 kHz.

The brightness temperature spectra for the different azimuth angles were simulated using the ARTS model. This forward model applies a vector radiative transfer code which includes the Zeeman effect. ARTS was set up with all the information about instrumental aspects and location of TEMPERA in order to simulate the same measurement conditions. These simulations showed almost identical spectra for most of the frequency range (4 MHz) and differences were only observed in the central part when the observational azimuth angle was changed. The spectra considering linear horizontal polarization showed lower values of brightness temperature and flatter shapes for the highest azimuth angles, while for lower angles the spectra showed higher values and the shapes were less flat. The maximum difference in brightness temperature between the most intensive spectrum (91.5°) and the least intensive (191.5°) was 2.5 K. For the linear vertical polarization the effect in the central frequencies was smaller, with a maximum difference of brightness temperature of 1 K between the most and the least intensive spectra; the azimuthal order was the inverse. These results are an evidence of the polarized nature associated with the Zeeman effect, which shows changes in the polarized state of the observed radiation when the angle between the propagation path and the direction of the Earth's magnetic field is varied.

In order to compare the ARTS simulations with the measurements the effects on the polarization state of the radiation due to the different optical components of TEMPERA radiometer were taken into account using the GRASP software package. The effective brightness temperature calculated after this correction showed that the most intense and least-broad spectrum was found at 71.5° and the least intense and most-broad spectrum was found at 131.5°. The maximum difference between both spectra was 2.3 K.

Similar behavior to the simulations was observed for the measured spectra from the TEMPERA radiometer. A direct comparison of the ratios of the maximum brightness temperature of each spectrum to the mean value for all the spectra at the central frequencies showed a very good agreement between the model and the measurements. Both simulations and measurements showed a smaller broadening for the smallest azimuth angles and a larger broadening for the largest angles. The small discrepancies found for some azimuth angles were always within of the measurement uncertainties.

This comparison is so far the most stringent test of the implementation of the Zeeman effect in ARTS. The comparison provides an effective test for the first three components of the Stokes vector. The third component, U, affects the end result through the rotation in Eq. (5). For example, if U were treated to be 0, this would give a clear degradation of the match between ARTS and TEMPERA in Fig. 11. ARTS is presently compared to a Zeeman forward model developed especially for handling circularly polarized radiation, providing a test for the last Stokes component.

The inclusion of the Zeeman effect in the ARTS model will allow extension of the upper limit of temperature profiles from ground-based microwave radiometers beyond 50 km. Preliminary results of the temperature retrievals including the Zeeman effect show higher values of the measurement response at higher altitudes, indicating a possible extension of several kilometers of the temperature profiles. This new retrieval setup and a detailed validation of the temperature profiles will be presented in a separate paper.

It has also the potential for improving the temperature retrieval for stratospheric and mesospheric T sounders onboard satellites. A related application is the assimilation of Zeeman affected brightness temperatures into NWP models, where ARTS can help to assess the accuracy of the more approximate, but much faster, radiative transfer tools applied for that purpose.

Acknowledgements. This work has been funded by the Swiss National Science Foundation under grant 200020-146388 and MeteoSwiss in the framework of the GAW project "Fundamental GAW Parameters by Microwave Radiometry".

Edited by: B. Funke

References

Buehler, S. A., Eriksson, P., Kuhn, T., Von Engeln, A., and Verdes, C.: ARTS, the atmospheric radiative transfer simulator, J. Quant. Spectrosc. Ra., 91, 65–93, 2005.

Christensen, H. and Veseth, L.: On the high-precision zeeman effect in O_2 and SO, J. Mol. Spectrosc., 72, 438–444, 1978.

Del Toro Iniesta, J. C.: Introduction to Spectropolarimetry, Cambridge University Press, UK, ISBN 0-521-81827-3, 2003.

Eriksson, P., Ekström, M., Melsheimer, C., and Buehler, S. A.: Efficient forward modelling by matrix representation of sensor responses, Int. J. Remote Sens., 27, 1793–1808, 2006.

Eriksson, P., Buehler, S. A., Davis, C. P., Emde, C., and Lemke, O.: ARTS, the atmospheric radiative transfer simulator, version 2, J. Quant. Spectrosc. Ra., 112, 1551–1558, 2011.

Forkman, P., Christensen, O. M., Eriksson, P., Urban, J., and Funke, B.: Six years of mesospheric CO estimated from ground-based frequency-switched microwave radiometry at 57° N compared with satellite instruments, Atmos. Meas. Tech., 5, 2827–2841, doi:10.5194/amt-5-2827-2012, 2012.

Gautier, D.: Influence du champ magnetique terrestre sur le transfert du rayonnement millimetrique dans l'oxygene moleculaire de l'atmosphere, Ann. Geophys., 23, 535–568, 1967, http://www.ann-geophys.net/23/535/1967/.

Gush, H. P., Halpern, M., and Wishnow, E. H.: Rocket measurement of the cosmic-background-radiation mm-wave spectrum, Phys. Rev. Lett., 65, 537–540, 1990.

Han, Y., Weng, F., Liu, Q., and van Delst, P.: A fast radiative transfer model for SSMIS upper atmosphere sounding channels, J. Geophys. Res.-Atmos. (1984–2012), 112, D11121, doi:10.1029/2006JD008208, 2007.

Han, Y., van Delst, P., and Weng, F.: An improved fast radiative transfer model for special sensor microwave imager/sounder upper atmosphere sounding channels, J. Geophys. Res.-Atmos. (1984–2012), 115, D15109, doi:10.1029/2010JD013878, 2010.

Hartmann, G. K., Degenhardt, W., Richards, M. L., Liebe, H. J., Hufford, G. A., Cotton, M. G., Bevilacqua, R. M., Olivero, J. J., Kämpfer, N., and Langen, J.: Zeeman splitting of the 61 Gigahertz Oxygen (O_2) line in the mesosphere, Geophys. Res. Lett., 23, 2329–2332, 1996.

Hoppel, K. W., Eckermann, S. D., Coy, L., Nedoluha, G. E., Allen, D. R., Swadley, S. D., and Baker, N. L.: Evaluation of SSMIS upper atmosphere sounding channels for high-altitude data assimilation, Mon. Weather Rev., 141, 3314–3330, 2013.

Ingold, T., Peter, R., and Kämpfer, N.: Weighted mean tropospheric temperature and transmittance determination at millimeter-wave frequencies for groundbased applications, Radio Sci., 33, 905–918, 1998.

Larsson, R., Buehler, S. A., Eriksson, P., and Mendrok, J.: A treatment of the Zeeman effect using Stokes formalism and its implementation in the Atmospheric Radiative Transfer Simulator (ARTS), J. Quant. Spectrosc. Ra., 133, 445–453, 2014.

Lenoir, W. B.: Propagation of partially polarized waves in a slightly anisotropic medium, J. Appl. Phys., 38, 5283–5290, 1967.

Lenoir, W. B.: Microwave spectrum of molecular oxygen in the mesosphere, J. Geophys. Res., 73, 361–376, 1968.

Liou, K. N.: An Introduction to Atmospheric Radiation, 2nd Edn., Academic Press, London, UK, 2002.

Navas-Guzmán, F., Stähli, O., and Kämpfer, N.: An integrated approach toward the incorporation of clouds in the temperature retrievals from microwave measurements, Atmos. Meas. Tech., 7, 1619–1628, doi:10.5194/amt-7-1619-2014, 2014.

Pardo, J. R., Pagani, L., Gerin, M., and Prigent, C.: Evidence of the Zeeman splitting in the $2_1 \rightarrow 0_1$ rotational transition of the atmospheric $^{16}O\,^{18}O$ molecule from ground-based measurements, J. Quant. Spectrosc. Ra., 54, 931–943, 1995.

Rosenkranz, P. W.: Absorption of microwaves by atmospheric gases, in: Atmospheric Remote Sensing by Microwave Radiometry, edited by: M. A. Janssen, Wiley, New York, NY, USA, available at: http://hdl.handle.net/1721.1/68611, 1993.

Rosenkranz, P. W. and Staelin, D. H.: Polarized thermal microwave emission from oxygen in the mesosphere, Radio Sci., 23, 721–729, 1988.

Rothman, L. S., Gordon, I. E., Babikov, Y., Barbe, A., Chris Benner, D., Bernath, P. F., Birk, M., Bizzocchi, L., Boudon, V., Brown, L. R., Campargue, A., Chance, K., Cohen, E. A., Coudert, L. H., Devi, V. M., Drouin, B. J., Fayt, A., Flaud, J.-M., Gamache, R. R., Harrison, J. J., Hartmann, J.-M., Hill, C., Hodges, J. T., Jacquemart, D., Jolly, A., Lamouroux J., Le Roy, R. J., Li,

G., Long, D. A., Lyulin, O. M., Mackie, C. J., Massie, S. T., Mikhailenko, S., Müller, H. S. P., Naumenko, O. V., Nikitin, A. V. Orphal, J., Perevalov, V., Perrin, A., Polovtseva, E. R., Richard, C., Smith, M. A. H., Starikova, E., Sung, K., Tashkun, S., Tennyson, J., Toon, G. C., Tyuterev, V. G., and Wagner, G.: The HITRAN2012 molecular spectroscopic database, J. Quant. Spectrosc. Ra., 130, 4–50, 2013.

Schwartz, M. J., Read, W. G., and Van Snyder, W.: EOS MLS forward model polarized radiative transfer for Zeeman-split oxygen lines, IEEE T. Geosci. Remote, 44, 1182–1191, 2006.

Shvetsov, A. A., Fedoseev, L. I., Karashtin, D. A., Bol'shakov, O. S., Mukhin, D. N., Skalyga, N. K., and Feigin, A. M.: Measurement of the middle-atmosphere temperature profile using a ground-based spectroradiometer facility, Radiophys. Quantum El., 53, 321–325, 2010.

Stähli, O., Murk, A., Kämpfer, N., Mätzler, C., and Eriksson, P.: Microwave radiometer to retrieve temperature profiles from the surface to the stratopause, Atmos. Meas. Tech., 6, 2477–2494, doi:10.5194/amt-6-2477-2013, 2013.

Von Engeln, A. and Buehler, S. A.: Temperature profile determination from microwave oxygen emissions in limb sounding geometry, J. Geophys. Res., 107, 4395, doi:10.1029/2001JD001029, 2002.

Von Engeln, A., Buehler, S. A., Langen, J., Wehr, T., and Kuenzi, K.: Retrieval of upper stratospheric and mesospheric temperature profiles from Millimeter-Wave Atmospheric Sounder data, J. Geophys. Res., 103, 31735–31748, 1998.

Waters, J. W.: Ground-based measurement of millimetre-wavelength emission by upper stratospheric O_2, Nature, 242, 506–508, 1973.

Zeeman, P.: On the Influence of Magnetism on the Nature of the Light Emitted by a Substance, Astrophys. J., 5, 332–347, 1897.